Geophysical Research Letters®

Key Points:
- Subsea permafrost degradation was up to 170% faster below submerged thermokarst basins compared to submerged Yedoma remnants nearshore
- Re-worked permafrost beneath thermokarst basins adjacent to lagoons induces rapid offshore thaw
- Along the assessed Arctic coastline, 54% of lagoons originated in thermokarst basins

Onshore Thermokarst Primes Subsea Permafrost Degradation

Michael Angelopoulos[1,2], Pier P. Overduin[1], Maren Jenrich[1,2], Ingmar Nitze[1], Frank Günther[2], Jens Strauss[1], Sebastian Westermann[3], Lutz Schirrmeister[1], Alexander Kholodov[4,5], Michael Krautblatter[6], Mikhail N. Grigoriev[7], and Guido Grosse[1,2]

[1]Permafrost Research Section, Alfred Wegener Institute Helmholtz Centre for Polar and Marine Research, Potsdam, Germany, [2]Institute of Geosciences, University of Potsdam, Potsdam, Germany, [3]Department of Geosciences, University of Oslo, Oslo, Norway, [4]Geophysical Institute, University of Alaska Fairbanks, Fairbanks, AK, USA, [5]Institute of Physical-Chemical and Biological Problems of Soil Science, Russian Academy of Sciences, Pushchino, Russia, [6]Department of Civil, Geo, and Environmental Engineering, Technical University of Munich, Munich, Germany, [7]Melnikov Permafrost Institute, Siberian Branch of the Russian Academy of Sciences, Yakutsk, Russia

Abstract The response of permafrost to marine submergence can vary between ice-rich late Pleistocene deposits and the thermokarst basins that thawed out during the Holocene. We hypothesize that inundated Alases offshore thaw faster than submerged Yedoma. To test this hypothesis, we estimated depths to the top of ice-bearing permafrost offshore of the Bykovsky Peninsula in northeastern Siberia using electrical resistivity surveys. The surveys traversed submerged lagoon deposits, drained and refrozen Alas deposits, and undisturbed Yedoma from the coastline to 373 m offshore. While the permafrost degradation rates of the submerged Yedoma were in the range of similar sites, the submerged Alas permafrost degradation rates were up to 170% faster. Remote sensing analyses suggest that 54% of lagoons wider than 500 m along northeast Siberian and northwest American coasts originated in thermokarst basins. Given the abundance of thermokarst basins and lakes along parts of the Arctic coastline, their effect on subsea permafrost degradation must be similarly prevalent.

Plain Language Summary Permafrost is defined as any ground or rock colder than 0°C for two or more consecutive years. In unglaciated regions of Siberia during the last ice age, the ground froze 1 km deep. When the ice sheets and glaciers melted at the end of the last Ice Age, millions of square kilometers of this cold permafrost were inundated with seawater on shallow Arctic shelves, creating subsea permafrost. Even today, new permafrost is submerged because of coastal erosion. Once submerged, heat and salt flow thaw the permafrost. However, the rate of subsea permafrost thaw partially depends on its temperature, ice content, and sediment type. Some permafrost areas called Alases already experienced deep thaw and refreezing from Arctic lake formation and drainage. On the southern coastline of the Bykovsky Peninsula in Siberia, we carried out non-invasive marine geophysical surveys parallel to the coastline to estimate how fast permafrost thaws beneath a submerged Alas next to a lagoon and permafrost areas without Alases. We discovered that subsea permafrost degradation was up to 170% faster beneath the submerged Alas nearshore. To highlight the broader relevance of these Alas-lagoon landscapes along the Arctic coastline, we map out Arctic lagoons.

1. Introduction

Subsea permafrost degradation rates are poorly constrained, mostly because we lack observational data. However, numerous modeling studies demonstrate that the degradation rate varies with sediment properties and porewater salinity (Frederick & Buffett, 2015; Nicolsky & Shakhova, 2010; Nicolsky et al., 2012; Overduin et al., 2019) and bottom water conditions (Dmitrenko et al., 2011; Golubeva et al., 2018; Harrison & Osterkamp, 1978). Repeated borehole observations close to the mouth of the Lena River suggest that degradation rates since the 1980s are increasing (Shakhova et al., 2017), which may have implications for shallow gas and carbon entrapped in ice-bearing permafrost (IBP) or shallow metastable inter-pore gas hydrates (Shakhova et al., 2019). Gas released from the dissociation of gas hydrates must bypass numerous physical and microbial sinks. Analyses of atmospheric methane fluxes (Kirschke et al., 2013; Saunois et al., 2020)

and global hydrate distribution (Ruppel, 2015) rule out subsea permafrost-associated gas hydrate forcing for currently observed climate warming (Ruppel & Kessler, 2017). Therefore, the mobilization of subsea permafrost organic carbon could be of greater importance (Sayedi et al., 2020; Wild et al., 2018).

Thermokarst is the process by which the thawing of ice-rich permafrost creates new landforms. These landforms are often depressions occupied by *thermokarst lakes*. When these lakes drain, the resulting topographic lows are called *Alases*. Thermokarst lakes and Alases become part of the marine environment because of transgressions and ingressions (Grosse et al., 2007) or through the development of channels (Romanovskii et al., 2000). If a thermokarst lake does not completely drain during the land to sea transition, then the talik underneath the lake can refreeze if a negative temperature profile develops in the sediment (Romanovskii et al., 2000). However, the newly formed frozen sediment can re-thaw later as the chemical degradation lags behind sediment refreezing (Angelopoulos, Overduin, Westermann, et al., 2020). Submerged thermokarst lake taliks may facilitate open talik development for gas migration (Frederick & Buffett, 2014). Nicolsky et al. (2012) modeled subsea permafrost on the East Siberian Arctic Shelf for the last several glacial cycles and demonstrated that open taliks can develop beneath thermokarst depressions in sediments with low porosity or in fault zones with high geothermal heat fluxes.

When thermokarst lakes drain, taliks can refreeze quickly under sub-aerial conditions, as much as 53 m in 157 yr (Ling & Zhang, 2004). O'Neill et al. (2020) provide a review of recent terrestrial talik research (2010–2019) and key terminology. Loss of high Pleistocene ground ice contents through thermokarst is generally not replaced by Holocene ice re-accumulation (Jorgenson & Shur, 2007). Therefore, relatively young drained lake basins have different permafrost characteristics compared to Yedoma remnants. For example, Alas deposits can hold three times more organic carbon per unit volume compared to Yedoma deposits (Jongejans et al., 2018) and trap large amounts of methane (Kraev et al., 2019). The high organic carbon contents are concentrated in lacustrine deposits, while the underlying taberal deposits tend to contain less organic carbon per unit volume than the original Yedoma (Kholodov et al., 2003; Shmelev et al., 2017). Snow can accumulate in topographic lows, leading to warmer ground temperatures (Kaverin et al., 2018). In cryopeg formations beneath a migrating river channel in northern Alaska, Stephani et al. (2020) showed that the epigenetic permafrost that formed beneath freshly exposed surfaces was ice-poor. However, the total volumetric ice content in an old Alas can be similar to that of Yedoma deposits due to large amounts of pore and segregated ice, especially in northeastern Siberia (Strauss et al., 2013; Ulrich et al., 2014). The altered latent heat content in Alas-permafrost can affect thawing rates for the next thermokarst phase. This hysteresis has been demonstrated in the modeling of thaw/refreeze cycles for onshore permafrost (Eliseev et al., 2014). Depending on its age, Alas-permafrost can be warmer, less ice-rich, and potentially more organic carbon-rich.

In this study, the term *Yedoma* is used to describe ice-rich Pleistocene permafrost deposits with syngenetic ice wedges where an Alas has not formed (Strauss et al., 2017). Electrical resistivity surveying has been successfully applied to map the top of subsea IBP (Angelopoulos et al., 2019; Overduin et al., 2012, 2016; Sellmann et al., 1989), onshore cryopegs connected to sub-lagoon taliks (Pedrazas et al., 2020), and seawater intrusion beneath the base of thin coastal permafrost (Kasprzak et al., 2017). Offshore, former lake basins infilled with sediment were detected with seismic methods (Portnov et al., 2018; Rekant et al., 2015) and transient electromagnetic surveys detected the top of subsea IBP and possibly deep paleo-taliks beneath submerged thermokarst (Shakhova et al., 2017). In this study, we applied marine electrical resistivity surveying to test the following hypothesis: *Alas permafrost landscapes submerged by seawater are pre-conditioned to degrade faster than previously undisturbed Yedoma permafrost deposits.* The results have implications for subsea permafrost on Arctic shelves and along coastal stretches with abundant thermokarst terrain.

2. Study Area

The fieldwork took place on the Bykovsky Peninsula's southern coastline in northeastern Siberia in July 2017. Thermokarst processes here have a major impact on the landscape and lakes alone characterize approximately 15% of the peninsula (Grosse et al., 2008). Including drained lake basins, thermokarst-affected landscapes exceed 50% of the total land area (Grosse et al., 2005). Approximately 23% of the coastline is dominated by Alas terrain and 13% by sand bar or lagoon barriers (Lantuit, Atkinson, et al., 2011). Between

1951 and 2006, the mean erosion rate was more than twice as fast for Alas coastlines compared to Yedoma, possibly due to lower ice content and a lower cliff height to erode. However, the differential erosion rate can create embayments that reduce hydrodynamic forcing along Alas coastlines. Then, the erosion rate along Alas coastlines can decrease. The balance of these processes may explain why the Alas coastline is not further inland than the Yedoma for the southern coastline.

3. Methods

In our study area, we aimed to quantify relative thaw rates of the different terrain units once submerged, providing an insight into the priming of subsea permafrost degradation by prior thermokarst lagoon development along the Arctic coast. To quantify the abundance of these features, we mapped thermokarst lagoons along Arctic coasts in the Canadian and Alaskan Chukchi and Beaufort seas, as well as the northeastern Siberian seas.

3.1. Arctic Lagoon Mapping and Remote Sensing

We manually mapped the number and distribution of lagoons wider than 500 m along the Arctic coast from the Taimyr Peninsula in Russia to the Tuktoyaktuk Peninsula in Canada. Our study area includes the Laptev, East Siberian, Chukchi, and Beaufort sea coasts. The mapping was conducted in Google Earth Engine and QGIS3.6 using Sentinel-2 imagery. We created a mosaic covering the entire coastal study domain and consisting of August–September 2018 median pixel values for a false color near-infrared, red, green band combination (8-4-3) at 10 m pixel resolution. We visually identified thermokarst lagoons according to the following criteria:

1. Located in a thermokarst environment
2. Had a round to oval-shaped depression with a discernible shoreline
3. At least intermittent connection with the sea through (a) a visible channel with a maximum length of 1 km, (b) separation only by a narrow sand barrier; or (c) high likelihood of regular water exchange via spring tides or storm surges if the maximum elevation difference to the sea is <1.5 m.

Elevation differences between land and sea were measured using the ArcticDEM digital elevation model (DEM) and its hillshade (HSarcticDEM) (Porter et al., 2018). In the Sentinel Hub Playground (https://apps.sentinel-hub.com/sentinel-playground) the "Moisture Index" (band combination $(B8A - B11)/(B8A + B11)$) and "Geology" layers (band combination 12-4-2) were used to visually determine the nature of barriers between coastal water bodies and the sea. Interconnected lagoons were defined as one system.

3.2. Electrical Resistivity Surveys

We performed four electrical resistivity surveys parallel to the southern coastline of the Bykovsky Peninsula in July 2017 (Figure 1). We extrapolated all onshore terrain units to offshore and assumed that our offshore surveys parallel to shore traversed all the units. An additional transect perpendicular to the Yedoma shoreline combined with a terrestrial survey is presented in Angelopoulos et al. (2019). The profiles were collected with an IRIS Syscal Pro Deep Marine system. The system was equipped with an echo-sounder to measure water depths and apparent resistivity data was collected approximately every 5 m. The geoelectric cable consisted of two current electrodes and eleven potential electrodes arranged in a reciprocal Wenner-Schlumberger array with a 10 m electrode separation. The array was quasi-symmetrical and each vertical sounding had alternate electrode pairs that were slightly off center. Ten apparent resistivity readings were taken at each sounding location. Conductivity, depth, and temperature casts were taken to constrain the water layer resistivity in the inversions. The depth to IBP was interpreted where the maximum rate of change of the natural logarithm of inverted resistivity vs. depth occurred. The depth of investigation (DOI) provides an estimate of the depth to which the inverted electrical resistivity can be considered reliable (Vest Christiansen & Auken, 2012). The laterally constrained 1D inversions (Auken et al., 2005) and IBP determination are described in the Supporting Information.
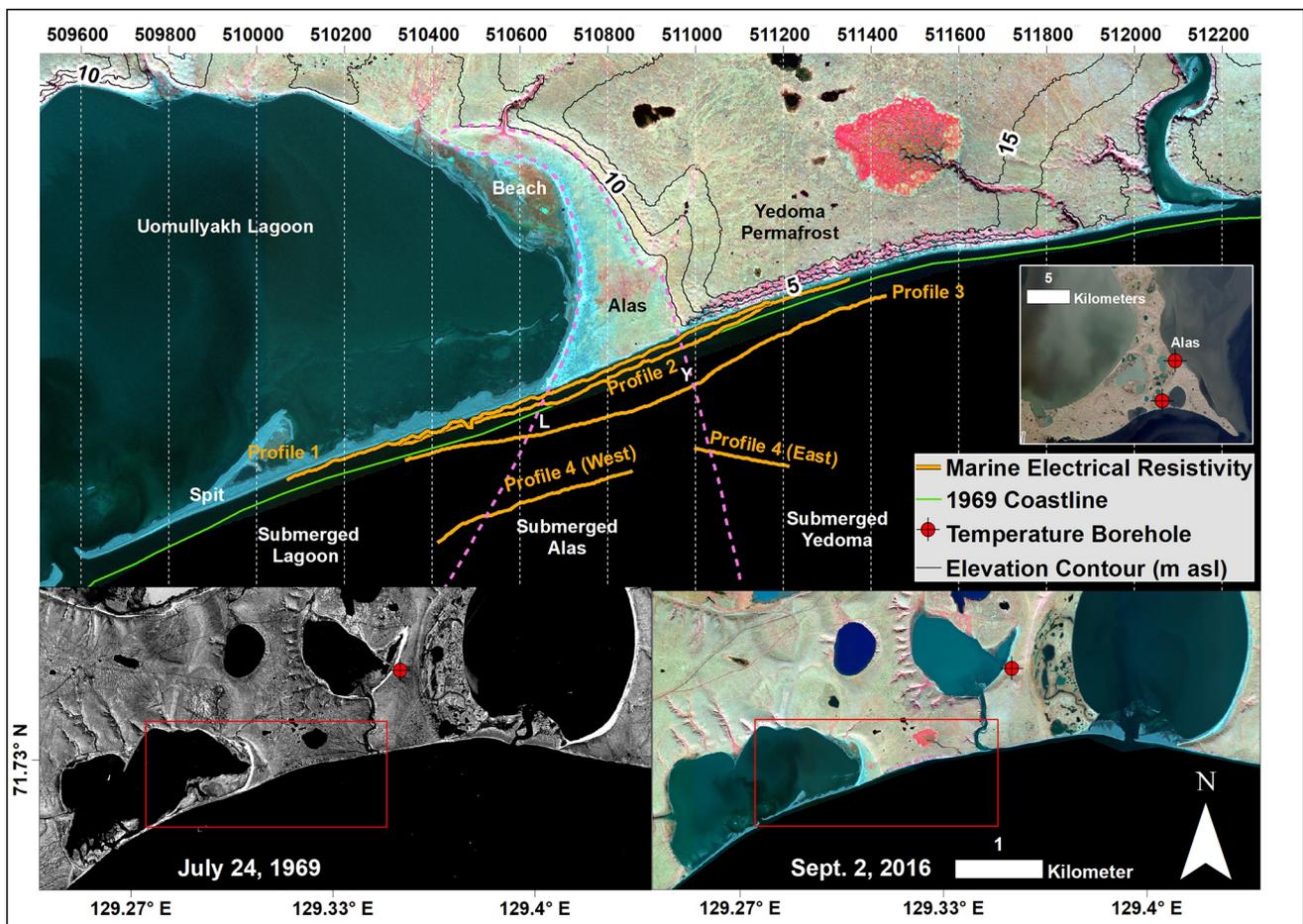
Figure 1. Top: Electrical resistivity survey locations from July 2017 superimposed on a high resolution satellite image (30 cm ground resolution WorldView-3 image from September 2, 2016 (DigitalGlobe©)). For context, the 1969 coastline and Yedoma temperature borehole (Schirrmeister et al., 2018) are also shown. The lagoon/Alas and Alas/Yedoma boundaries are extrapolated offshore and denoted "L" and "Y" respectively in Figure 3. To ease interpretation of the electrical resistivity profiles (Figure 3), easting (m) indicators are shown every 200 m. Bottom left: 1969 CORONA satellite image of the study area with the fieldwork map extent outline in the red rectangle. This is preferentially shown instead of an image available from 1951 because of better resolution. Bottom right: 2016 satellite image (WorldView-3) of the study area with the fieldwork map extent outline in the red rectangle.

4. Results

4.1. Arctic Lagoon Mapping and Remote Sensing

Of all 469 mapped lagoons, 253 (54%) originated in thermokarst basins (Figure 2). Most of the thermokarst lagoons (117) were located along the Beaufort Sea coastline. Along the coast of the Laptev Sea, 81 lagoons were mapped, 20 of which were thermokarst lagoons. In addition, all lagoons identified in the Lena River Delta originated from tapped thermokarst lakes. The observations showed that thermokarst lagoons were mainly restricted to lowland areas and were most abundant in delta regions. Six lagoons were identified on the Bykovsky Peninsula, all of them located in the south of the peninsula. Five of the six originated from thermokarst basins. Figure S1 shows all 469 lagoons mapped along the Arctic coast between the Taimyr Peninsula and the Tuktoyaktuk Peninsula west of the Mackenzie Delta. The Beaufort Sea coast featured the most lagoons (153), but was also the longest coastline investigated.

4.2. Submerged Yedoma Deposits

Offshore of the Bykovsky Peninsula's southern coastline, the most highly resistive subsurface layers were observed beneath submerged Yedoma (Figure 3). For each profile, there was a clear lateral transition in resistivity and depth to IBP at the submerged Alas/Yedoma transition. Similar to Angelopoulos et al. (2019),

Figure 2. Arctic coastline map of the 253 thermokarst lagoons along the Arctic coast between the Taimyr Peninsula (Siberia) and the Tuktoyaktuk Peninsula (Northwest Territories, Canada); number of lagoons in brackets.

the transition to IBP occurred between 16 and 130 Ωm. Within the frozen sediment body, the resistivity increased to 250 Ωm for profiles 1 and 2, but exceeded 500 Ωm for profile 3. For profile 3, the DOI was slightly below the depth to IBP and above the highly resistive zone in the submerged Yedoma. Along profile 4, the farthest from shore, the maximum resistivity of the IBP was only 75 Ωm. The depth to IBP increased from 1 to 2 m within 10 m of the coastline, to 8 m at 110 m offshore, and finally to 12 m at 300 m from the shoreline (Figure S2).

4.3. Submerged Alas and Lagoon Deposits

For profile 1, there was a clear distinction between the submerged Alas and the submerged lagoon deposits. Beginning at the submerged Alas/Yedoma boundary, the depth to IBP increased from approximately 5 to 15 m toward the lagoon/Alas boundary (Figure 3). Beneath the submerged lagoon deposits, the depth to IBP increased with distance away from the Alas. Furthermore, the unfrozen to frozen transition occurred at a
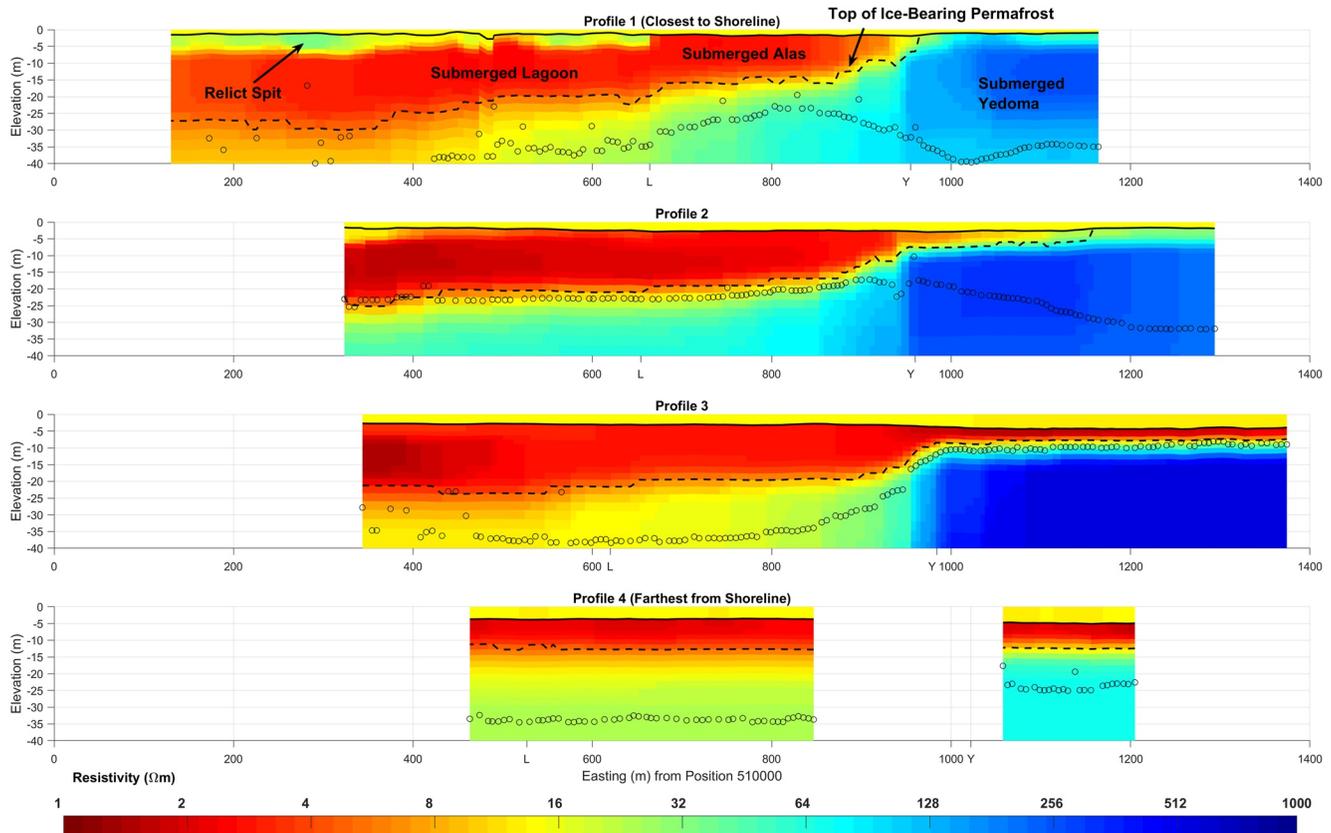
Figure 3. Electrical resistivity of four surveys parallel to shore in July 2017. The surveys traverse submerged lagoon, as well as submerged Alas and Yedoma terrain. The boundaries between each unit were extrapolated offshore as shown in Figure 1. On the *X* axis of the profiles, "L" denotes the lagoon to Alas boundary and "Y" the Alas to Yedoma boundary. The thick black line is the water depth, the dotted black line is the interpreted depth to the top of ice-bearing permafrost (IBP), and the black circles indicate the depth of investigation (DOI).

lower resistivity (around 8 Ωm) compared to the submerged Alas and Yedoma. In addition, a relatively high resistivity feature (up to 30 Ωm) 5 m thick was detected just below the seabed for the submerged lagoon. For both the Alas and the lagoon, the depth to IBP was above the DOI. Along profile 2, both the Alas and lagoon segments were similar. From the westernmost edge of the survey line to 800 m, the depth to IBP was 19 m and the frozen sediment had a maximum resistivity of 75 Ωm. The depth to IBP was slightly above the DOI for most of the profile west of the Yedoma. Along profile 3, the depth to IBP was 19 m in the Alas and as deep as 24 m in the lagoon, but the profile drifted toward the shoreline past the lagoon boundary (Figure 1). For both submerged landscape units, the depth to IBP was above the DOI. For profile 4, the IBP depth was 12 m in both the submerged lagoon and Alas. While the resistivity at the unfrozen to frozen interface was similar to profile 3, the depth to IBP was shallower despite being more than 100 m further offshore. The data residual for each sounding of all profiles was less than 1.0 assuming an uncertainty level of 5% on the apparent resistivity.

Overall, there was a strong linear fit between IBP depth and the natural logarithm of offshore distances less than 120 m for the Alas, but not for the lagoon, which yielded a negative correlation (Figure S2). When considering the natural logarithm of all offshore distances, both landscape units yielded weak linear fits with IBP depths. For coastal erosion rates of 0.25 and 0.50 m/yr, the maximum IBP degradation rate was 0.16–0.32 m/yr for the Alas at a 30 m offshore distance compared to 0.06–0.12 m/yr for Yedoma, representing an increase of up to 170% for the Alas. This disparity was present up to 120 m from shore.

5. Discussion

The depth to IBP beneath submerged Yedoma increased logarithmically with distance offshore and thus inundation time. The warm discharge of the Lena River results in faster IBP degradation rates in this area compared to the western Laptev Sea (Angelopoulos, Overduin, Miesner, et al., 2020). Since the coastline cuts approximately perpendicular across terrain unit boundaries, relative differences in degradation rates between submerged Yedoma and Alas therefore hold, irrespective of the coastal erosion rate. As shown in Figure 1, the 1969 coastline intersects profile 2, showing that the Alas was submerged after coastal erosion. The coastal erosion rate was approximately 0.5 m/yr for the Alas coastline from 1969 to 2017, corresponding to 48 yr of inundation. For further offshore distances (profiles 3 and 4), there is more uncertainty regarding the lagoon/Alas and Alas/Yedoma boundaries, as well as the Alas inundation history. Lower lying Alases could have been submerged earlier from rising sea levels (Gavrilov et al., 2006; Romanovskii et al., 2000), but this does not contradict the high rate of subsea IBP degradation for the submerged Alas deposits close to shore (up to 19 m in 48 yr). Shakhova et al. (2017) showed that the depth to IBP for submerged Yedoma permafrost offshore of Muostakh Island's north tip increased from 4.2 m after 49 yr of inundation (1982 borehole) to 8.6 m after 81 yr of inundation (2014 borehole).

The high rate of subsea IBP degradation for submerged Alas deposits within 30 m of the coastline suggests that conditions prior to submergence favor thawing. This may be partially due to a warmer ground thermal regime upon submergence, as borehole measurements showed that the average ground surface temperature in an Alas depression from 2012 to 2015 was −7°C compared to −10°C for Yedoma (Figure S3). However, this effect is less important than the reduced latent heat content associated with relatively ice-poor refrozen talik deposits. In this region, the total ice content (segregated ice + wedge ice) can reach up to 87% by volume for Yedoma deposits (Fuchs et al., 2020; Günther et al., 2015). The Alas had been sub-aerially exposed since at least 1951 (year of oldest available image), but partial lake drainage and lagoon formation likely occurred centuries earlier (Jenrich et al., 2021). The Stefan solution for permafrost formation (Riseborough et al., 2008) yields a sub-aerial refrozen talik down to 21 m in just 66 yr and 37 m in 200 yr, using a ground temperature of −7°C, a volumetric ice content of 50%, and a frozen sediment thermal conductivity of 2.6 W/(mK). The conductivity is representative for sediment in the East Siberian Arctic seas (Chuvilin et al., 2020). We conclude that the deep IBP (19 m within 30 m of shore) is indicative of marine-induced thaw and not relict thaw from the original thermokarst lake. We further suggest that in addition to warmer sediment temperatures and potentially low ice contents in the Alas, salt intrusion from lagoon-Alas interaction could precondition the sediment for rapid thaw.

Lateral seawater intrusion beneath a thin permafrost base was interpreted by electrical resistivity surveys several decameters inland in Svalbard (Kasprzak et al., 2017), leading to the concept of an onshore-permafrost wedge (Kasprzak, 2020). Due to seawater intrusion, this concept explains that the thickness of onshore permafrost increases with distance from the coastline. On the Bykovsky Peninsula, we suspect that lateral saltwater intrusion from the lagoon occurred beneath the sub-aerial Alas during refreezing. The driftwood on the Alas surface (Figure 1) indicates that it is also susceptible to storm surges and tidal flooding from the lagoon. A borehole drilled in the center of Uomullyakh Lagoon in April 2017 showed unfrozen hypersaline sediment down to a depth of 20 m below the top of the bedfast ice (1.2 m thick), despite temperatures as low as −4.4°C (Jenrich et al., 2021). Below 20 m, the temperature was as cold as −5.0°C and below the freezing point estimated from porewater electrical conductivity. The nearly uniform salt distribution vs. depth is not indicative of slow vertical diffusive salt transport (Harrison & Osterkamp, 1982). The Alas is part of the same basin and should have similar sediment properties conducive to density-driven water flow. The depth to IBP in the borehole was deeper than the maximum depth of the Yedoma (15 m below sea level), indicating that all the massive ice melted during the thermokarst lake phase. The IBP discovered in the borehole was characterized by sands underlying the Yedoma. Although remnants of the Yedoma can exist below drained lake basins (Kholodov et al., 2003), the lower resistivity of the IBP below the Alas deposits compared to Yedoma indicates that the submerged Yedoma IBP has a higher ice content than the Alas IBP. The lateral intrusion of saltwater into an Alas that starts to refreeze could create saline sub-aerial permafrost and cryopegs. Even if the saline Alas layers freeze, thawing would still be faster because of the reduced freezing point of the porewater and a higher unfrozen water content at temperatures below the freezing point (Nicolsky & Shakhova, 2010). The re-worked Alas deposits might also be more susceptible to convective salt

transport offshore. As observed in Prudhoe Bay, Alaska, the convective transport of salt to the phase boundary can greatly increase the subsea permafrost degradation rate (Osterkamp, 2001; Osterkamp et al., 1989).

The Alas IBP depth showed a strong linear fit with the natural logarithm of offshore distances, but only less than 120 m from shore. For offshore distances greater than 200 m, the depth to IBP in the Alas was only 12 m compared to 19 m for offshore distances between 90 and 120 m (Figure S2). This is possible because the terrain unit extrapolation shown in Figure 1 is more unreliable at large distances from shore. However, if the terrain unit extrapolation is correct, we attribute the aforementioned finding to the fact that the submerged Alas more than 200 m offshore was pre-conditioned with salt and low ice content to a shallower depth or not at all. After a partially frozen saline layer thaws, the IBP degradation rate slows considerably. At this point, numerical models suggest that the IBP can degrade from salt diffusion from the overlying saline sediment (Figure S4). After enough time, the 0°C isotherm will catch up to the thawing front to accelerate IBP degradation. In Tiksi Bay, the mean annual bottom water temperature is above 0°C. The thermal models are described in the supporting information and are based on CryoGrid2 (Westermann et al., 2013) adapted for salt diffusion (Angelopoulos et al., 2019).

The interpreted IBP depths beneath the submerged lagoon were the deepest, based on the assumption that an unfrozen to frozen transition occurred at the maximum rate of change of the natural logarithm of inverted electrical resistivity vs. depth. It is possible that the transition was the shift from unfrozen saline ground to less saline, but still unfrozen ground. The very low resistivity transition to IBP (8 Ωm) is corroborated by Overduin et al. (2012) and Wu et al. (2017), who demonstrated that the bulk resistivity of hypersaline sediment can be 2–3 Ωm at the freezing point. Furthermore, IBP depths beneath the submerged lagoon were complicated by the spit, which moves along with the retreating coast. In profile 1, the high resistivity feature just below the seabed was likely relict IBP aggradation from the spit's position in earlier years. Cooling from the sub-aerially exposed spit could have also created permafrost upwards from the bottom of the talik. In the eastern Beaufort Sea, Ruppel et al. (2016) attributed shallower and thicker IBP to the presence of barrier islands. Permafrost aggradation also occurs below tidal flats, like in the Kara Sea (Vasiliev et al., 2017), as well as emerging polar coasts from isostatic rebound (Boisson et al., 2020). However, it is unlikely that the Alas was once submerged and uplifted, because the Bykovsky Peninsula lies in an area of tectonic subsidence (Morgenstern et al., 2020).

Spits and barrier islands may be important controls on subsea IBP preservation in the Arctic where large lagoons (>500 m) are widespread, like in the Beaufort Sea (Figure S1). The capacity for thermokarst-affected landscapes to increase subsea permafrost degradation is most significant where thermokarst lagoons and Alases interact with each other, such as along some stretches of the Laptev and Beaufort seas (Figure 2). Higher elevated Alas-rich coastlines with comparatively few lagoons like in Eastern Siberia may experience slower subsea permafrost degradation rates, but still thaw faster than Yedoma dominated coastal stretches.

6. Conclusions

We performed marine electrical resistivity surveys parallel to the southern coastline of the Bykovsky Peninsula to map the depth to the top of subsea IBP. The resistivity data indicate that the subsea permafrost degradation rate was up to 170% faster below submerged Alas deposits compared to submerged Yedoma permafrost. The deeper IBP table observed beneath submerged Alases adjacent to thermokarst lagoons is consistent with our hypothesis. While subsea permafrost thaw is generally slower than thaw beneath thermokarst lakes, reworked low-lying Alas deposits are primed for rapid degradation upon marine inundation. Arctic coastal erosion rates are also increasing, leading to faster inundation of terrestrial permafrost (Jones et al., 2018; Lantuit, Overduin, et al., 2011). The thermokarst lake phase can generate deep taliks that facilitate subsea open talik development through bottom-up thawing, providing conduits for gas migration from degrading gas hydrates (Malakhova, 2016; Malakhova & Eliseev, 2018). We suggest that low-lying thermokarst-affected landscapes adjacent to lagoons are susceptible to more rapid top-down thaw once they become part of the marine environment. While the more rapid thaw we observed occurred in the uppermost 20 m, subsea permafrost is estimated to contain 500 Gt of carbon not embedded in hydrates in the upper 25 m of sediment (Shakhova et al., 2010; Zimov et al., 2006). Given the abundance of thermokarst lagoons in this large portion of the Arctic, as revealed by our remote sensing effort, large-scale thermal assessments

of subsea permafrost should consider reworked sediments beneath thermokarst depressions in numerical models. The presence of salt in IBP reduces the energy required for phase change, and thus submerged refrozen marine sediments are also pre-conditioned to degrade faster than submerged Yedoma deposits. Along Arctic coastal stretches of ice-rich permafrost, young Alases with low ice content, as well as Alases lying in thermokarst lagoon basins, are potential hot spots for rapid subsea permafrost degradation.

Data Availability Statement

The PANGAEA portal provides access to the apparent electrical resistivity data and water depths (https://doi.pangaea.de/10.1594/PANGAEA.934169), as well as the KML files for the Arctic lagoon mapping (https://doi.pangaea.de/10.1594/PANGAEA.934158). The borehole temperature data is available from the Arctic Data Center Portal of the Geophysical Institute, University of Alaska Fairbanks. The Yedoma borehole data can be accessed from https://permafrost.gi.alaska.edu/site/by1 and the Alas borehole data from https://permafrost.gi.alaska.edu/site/by3.

References

Angelopoulos, M., Overduin, P. P., Miesner, F., Grigoriev, M. N., & Vasiliev, A. A. (2020). Recent advances in the study of Arctic submarine permafrost. *Permafrost and Periglacial Processes*, *31*(3), 442–453. https://doi.org/10.1002/ppp.2061

Angelopoulos, M., Overduin, P. P., Westermann, S., Tronicke, J., Strauss, J., Schirrmeister, L., et al. (2020). Thermokarst lake to lagoon transitions in eastern Siberia: Do submerged taliks refreeze? *Journal of Geophysical Research: Earth Surface*, *125*, e2019JF005424. https://doi.org/10.1029/2019JF005424

Angelopoulos, M., Westermann, S., Overduin, P., Faguet, A., Olenchenko, V., Grosse, G., & Grigoriev, M. N. (2019). Heat and salt flow in subsea permafrost modeled with CryoGrid2. *Journal of Geophysical Research: Earth Surface*, *124*(4), 920–937. https://doi.org/10.1029/2018JF004823

Auken, E., Christiansen, A. V., Jacobsen, B. H., Foged, N., & Sørensen, K. I. (2005). Piecewise 1D laterally constrained inversion of resistivity data. *Geophysical Prospecting*, *53*(4), 497–506. https://doi.org/10.1111/j.1365-2478.2005.00486.x

Boisson, A., Allard, M., & Sarrazin, D. (2020). Permafrost aggradation along the emerging eastern coast of Hudson Bay, Nunavik (northern Québec, Canada). *Permafrost and Periglacial Processes*, *31*(1), 128–140. https://doi.org/10.1002/ppp.2033

Chuvilin, E., Bukhanov, B., Grebenkin, S., Tumskoy, V., Shakhova, N., Dudarev, O., et al. (2020). Thermal properties of sediments in the East Siberian Arctic Seas: A case study in the Buor-Khaya Bay. *Marine and Petroleum Geology*, *123*, 104672. https://doi.org/10.1016/j.marpetgeo.2020.104672

Dmitrenko, I. A., Kirillov, S. A., Tremblay, L. B., Kassens, H., Anisimov, O. A., Lavrov, S. A., et al. (2011). Recent changes in shelf hydrography in the Siberian Arctic: Potential for subsea permafrost instability. *Journal of Geophysical Research*, *116*(C10), C10027. https://doi.org/10.1029/2011JC007218

Eliseev, A. V., Demchenko, P. F., Arzhanov, M. M., & Mokhov, I. I. (2014). Transient hysteresis of near-surface permafrost response to external forcing. *Climate Dynamics*, *42*(5–6), 1203–1215. https://doi.org/10.1007/s00382-013-1672-5

Frederick, J., & Buffett, B. (2014). Taliks in relict submarine permafrost and methane hydrate deposits: Pathways for gas escape under present and future conditions. *Journal of Geophysical Research: Earth Surface*, *119*(2), 106–122. https://doi.org/10.1002/2013JF002987

Frederick, J., & Buffett, B. (2015). Effects of submarine groundwater discharge on the present-day extent of relict submarine permafrost and gas hydrate stability on the Beaufort Sea continental shelf. *Journal of Geophysical Research: Earth Surface*, *120*(3), 417–432. https://doi.org/10.1002/2014JF003349

Fuchs, M., Nitze, I., Strauss, J., Günther, F., Wetterich, S., Kizyakov, A., et al. (2020). Rapid fluvio-thermal erosion of a Yedoma permafrost cliff in the Lena River Delta. *Frontiers of Earth Science*, *8*(336). https://doi.org/10.3389/feart.2020.00336

Gavrilov, A., Romanovskii, N., & Hubberten, H. (2006). Paleographic scenario of the postglacial transgression on the Laptev Sea shelf. *Kriosfera Zemli (Earth's Cryosphere)*, *10*(1), 39–50.

Golubeva, E., Platov, G., Malakhova, V., Kraineva, M., & Iakshina, D. (2018). Modelling the long-term and interannual variability in the Laptev Sea hydrography and subsea permafrost state. *Polarforschung*, *87*, 195–210.

Grosse, G., Romanovsky, V., Walter, K., Morgenstern, A., Lantuit, H., & Zimov, S. (2008). Distribution of thermokarst lakes and ponds at three Yedoma sites in Siberia. In D. Kane, & K. Hinkel (Eds.), *Proceedings: Ninth International Conference on Permafrost* (pp. 551–556). Institute of Northern Engineering, University of Alaska Fairbanks. Retrieved form https://epic.awi.de/id/eprint/19086/

Grosse, G., Schirrmeister, L., Kunitsky, V. V., & Hubberten, H.-W. (2005). The use of CORONA images in remote sensing of periglacial geomorphology: An illustration from the NE Siberian coast. *Permafrost and Periglacial Processes*, *16*(2), 163–172. https://doi.org/10.1002/ppp.509

Grosse, G., Schirrmeister, L., Siegert, C., Kunitsky, V. V., Slagoda, E. A., Andreev, A. A., & Dereviagyn, A. Y. (2007). Geological and geomorphological evolution of a sedimentary periglacial landscape in Northeast Siberia during the Late Quaternary. *Geomorphology*, *86*(1), 25–51. https://doi.org/10.1016/j.geomorph.2006.08.005

Günther, F., Overduin, P. P., Yakshina, I. A., Opel, T., Baranskaya, A. V., & Grigoriev, M. N. (2015). Observing Muostakh disappear: Permafrost thaw subsidence and erosion of a ground-ice-rich island in response to Arctic summer warming and sea ice reduction. *The Cryosphere*, *9*(1), 151–178. https://doi.org/10.5194/tc-9-151-2015

Harrison, W. D., & Osterkamp, T. E. (1978). Heat and mass transport processes in subsea permafrost 1. An analysis of molecular diffusion and its consequences. *Journal of Geophysical Research*, *83*(C9), 4707–4712. https://doi.org/10.1029/JC083iC09p04707

Harrison, W. D., & Osterkamp, T. E. (1982). Measurements of the electrical conductivity of interstitial water in submarine permafrost. In H. M. French (Ed.), *Proceedings of the Fourth Canadian Permafrost Conference* (pp. 229–237). National Research Council of Canada. Retrieved from http://pubs.aina.ucalgary.ca/cpc/CPC4-229.pdf

Jenrich, M., Angelopoulos, M., Grosse, G., Overduin, P. P., Schirrmeister, L., Nitze, I., et al. (2021). Thermokarst Lagoons: A Core-based Assessment of Depositional Characteristics and an Estimate of Carbon Pools on the Bykovsky Peninsula. *Frontiers in Earth Science*, *9*. https://doi.org/10.3389/feart.2021.637899

Jones, B. M., Farquharson, L. M., Baughman, C. A., Buzard, R. M., Arp, C. D., Grosse, G., et al. (2018). A decade of remotely sensed observations highlight complex processes linked to coastal permafrost bluff erosion in the Arctic. *Environmental Research Letters*, *13*(11), 115001. https://doi.org/10.1088/1748-9326/aae471

Jongejans, L. L., Strauss, J., Lenz, J., Peterse, F., Mangelsdorf, K., Fuchs, M., & Grosse, G. (2018). Organic matter characteristics in Yedoma and thermokarst deposits on Baldwin Peninsula, west Alaska. *Biogeosciences*, *15*(20), 6033–6048. https://doi.org/10.5194/bg-15-6033-2018

Jorgenson, M. T., & Shur, Y. (2007). Evolution of lakes and basins in northern Alaska and discussion of the thaw lake cycle. *Journal of Geophysical Research*, *112*(F2). F02S17. https://doi.org/10.1029/2006JF000531

Kasprzak, M. (2020). Seawater intrusion on the Arctic Coast (Svalbard): The concept of onshore-permafrost wedge. *Geosciences*, *10*(9), 349. https://doi.org/10.3390/geosciences10090349

Kasprzak, M., Strzelecki, M. C., Traczyk, A., Kondracka, M., Lim, M., & Krzysztof, M. (2017). On the potential for a bottom active layer below coastal permafrost: The impact of seawater on permafrost degradation imaged by electrical resistivity tomography (Hornsund, SW Spitsbergen). *Geomorphology*, *293*, 347–359. https://doi.org/10.1016/j.geomorph.2016.06.013

Kaverin, D. A., Melnichuk, E. B., Shiklomanov, N. I., Kakunov, N. B., Pastukhov, A. V., & Shiklomanov, A. N. (2018). Long-term changes in the ground thermal regime of an artificially drained thaw-lake basin in the Russian European north. *Permafrost and Periglacial Processes*, *29*(1), 49–59. https://doi.org/10.1002/ppp.1963

Kholodov, A., Rivkina, E., Gilichinsky, D., Fyodorov-Davydov, D., Gubin, S., Sorokovikov, V., et al. (2003). Estimation of the organic carbon input into Arctic Ocean due to erosion of Laptev and East-Siberian seashore. *Cryosphere Earth*, *7*(3), 3–12.

Kirschke, S., Bousquet, P., Ciais, P., Saunois, M., Canadell, J. G., Dlugokencky, E. J., et al. (2013). Three decades of global methane sources and sinks. *Nature Geoscience*, *6*(10), 813–823. https://doi.org/10.1038/ngeo1955

Kraev, G., Rivkina, E., Vishnivetskaya, T., Belonosov, A., van Huissteden, J., Kholodov, A., et al. (2019). Methane in gas shows from boreholes in epigenetic permafrost of Siberian Arctic. *Geosciences*, *9*(2), 67. https://doi.org/10.3390/geosciences9020067

Lantuit, H., Atkinson, D., Paul Overduin, P., Grigoriev, M., Rachold, V., Grosse, G., & Hubberten, H.-W. (2011). Coastal erosion dynamics on the permafrost-dominated Bykovsky Peninsula, north Siberia, 1951–2006. *Polar Research*, *30*(1), 7341. https://doi.org/10.3402/polar.v30i0.7341

Lantuit, H., Overduin, P. P., Couture, N., Wetterich, S., Aré, F., Atkinson, D., et al. (2011). The Arctic coastal dynamics database: A new classification scheme and statistics on Arctic permafrost coastlines. *Estuaries and Coasts*, *35*(2), 383–400. https://doi.org/10.1007/s12237-010-9362-6

Ling, F., & Zhang, T. (2004). Modeling study of talik freeze-up and permafrost response under drained thaw lakes on the Alaskan Arctic Coastal Plain. *Journal of Geophysical Research*, *109*(D1), D01111. https://doi.org/10.1029/2003JD003886

Malakhova, V. (2016). On the thermal influence of thermokarst lakes on the subsea permafrost evolution. In *22nd International Symposium on Atmospheric and Ocean Optics: Atmospheric Physics* (Vol. 10035). International Society for Optics and Photonics. https://doi.org/10.1117/12.2248714

Malakhova, V., & Eliseev, A. (2018). Influence of rift zones and thermokarst lakes on the formation of subaqueous permafrost and the stability zone of methane hydrates of the Laptev Sea shelf in the Pleistocene. *Ice and Snow*, *58*(2), 231–242. https://doi.org/10.15356/2076-6734-2018-2-231-242

Morgenstern, A., Overduin, P. P., Günther, F., Stettner, S., Ramage, J., Schirrmeister, L., et al. (2020). Thermo-erosional valleys in Siberian ice-rich permafrost. *Permafrost and periglacial processes*. *32*, 59–75. https://doi.org/10.1002/ppp.2087

Nicolsky, D., Romanovsky, V. E., Romanovskii, N. N., Kholodov, A. L., Shakhova, N. E., & Semiletov, I. P. (2012). Modeling sub-sea permafrost in the East Siberian Arctic Shelf: The Laptev Sea region. *Journal of Geophysical Research*, *117*(F3), F03028. https://doi.org/10.1029/2012JF002358

Nicolsky, D., & Shakhova, N. (2010). Modeling sub-sea permafrost in the East Siberian Arctic Shelf: The Dmitry Laptev strait. *Environmental Research Letters*, *5*, 015006. https://doi.org/10.1088/1748-9326/5/1/015006

O'Neill, H. B., Roy-Leveillee, P., Lebedeva, L., & Ling, F. (2020). Recent advances (2010–2019) in the study of taliks. *Permafrost and Periglacial Processes*. *31*, 346–357. https://doi.org/10.1002/ppp.2050

Osterkamp, T. E. (2001). Sub-sea permafrost. In J. H. Steele, S. A. Thorpe, & K. K. Turekian (Eds.), *Encyclopedia of ocean sciences* (Vol. 5, pp. 2902–2912). Academic Press. https://doi.org/10.1006/rwos.2001.0008

Osterkamp, T. E., Baker, G. C., Harrison, W. D., & Matava, T. (1989). Characteristics of the active layer and shallow subsea permafrost. *Journal of Geophysical Research*, *94*(CII), 16227–16236. https://doi.org/10.1029/JC094iC11p16227

Overduin, P. P., Schneider von Deimling, T., Miesner, F., Grigoriev, M., Ruppel, C., Vasiliev, A., et al. (2019). Submarine permafrost map in the Arctic modeled using 1D transient heat flux (SuPerMAP). *Journal of Geophysical Research: Oceans*, *124*(6), 3490–3507. https://doi.org/10.1029/2018JC014675

Overduin, P. P., Westermann, S., Yoshikawa, K., Haberlau, T. S., Romanovsky, V., & Wetterich, S. (2012). Geoelectric observations of the degradation of nearshore submarine permafrost at Barrow (Alaskan Beaufort Sea). *Journal of Geophysical Research: Earth Surface*, *117*(F2), F02004. https://doi.org/10.1029/2011JF002088

Overduin, P. P., Wetterich, S., Günther, F., Grigoriev, M. N., Grosse, G., Schirrmeister, L., et al. (2016). Coastal dynamics and submarine permafrost in shallow water of the central Laptev Sea, East Siberia. *The Cryosphere*, *10*(4), 1449–1462. https://doi.org/10.5194/tc-10-1449-2016

Pedrazas, M. N., Cardenas, M. B., Demir, C., Watson, J. A., Connolly, C. T., & McClelland, J. W. (2020). Absence of ice-bonded permafrost beneath an Arctic lagoon revealed by electrical geophysics. *Science Advances*, *6*(43), eabb5083. https://doi.org/10.1126/sciadv.abb5083

Porter, C., Morin, P., Howat, I., Noh, M.-J., Bates, B., Peterman, K., et al. (2018). *ArcticDEM, Harvard Dataverse, V1*. Polar Geospatial Center, University of Minnesota. Retrieved from https://www.pgc.umn.edu/data/arcticdem/ [accessed January 2019]

Portnov, A., Mienert, J., Winsborrow, M., Andreassen, K., Vadakkepuliyambatta, S., Semenov, P., & Gataullin, V. (2018). Shallow carbon storage in ancient buried thermokarst in the South Kara Sea. *Scientific Reports*, *8*, 2045–2322. https://doi.org/10.1038/s41598-018-32826-z

Rekant, P., Bauch, H. A., Schwenk, T., Portnov, A. D., Gusev, E., Spiess, R., et al. (2015). Evolution of subsea permafrost landscapes in Arctic Siberia since the Late Pleistocene: A synoptic insight from acoustic data of the Laptev Sea. *arktos*, *1*(1), 1–15. https://doi.org/10.1007/s41063-015-0011-y

Riseborough, D., Shiklomanov, N., Etzelmüller, B., Gruber, S., & Marchenko, S. (2008). Recent advances in permafrost modelling. *Permafrost and Periglacial Processes*, *19*(2), 137–156. https://doi.org/10.1002/ppp.615

Romanovskii, N. N., Hubberten, H.-W., Gavrilov, A. V., Tumskoy, V. E., Tipenko, G. S., Grigoriev, M. N., & Siegert, C. (2000). Thermokarst and land-ocean interactions, Laptev Sea region, Russia. *Permafrost and Periglacial Processes*, *11*, 137–152. https://doi.org/10.1002/1099-1530(200004/06)11:2<137::aid-ppp345>3.0.co;2-l

Ruppel, C. D. (2015). Permafrost-associated gas hydrate: Is it really approximately 1% of the global system? *Journal of Chemical & Engineering Data*, *60*, 429–436. https://doi.org/10.1021/je500770m

Ruppel, C. D., Herman, B. M., Brothers, L. L., & Hart, P. E. (2016). Subsea ice-bearing permafrost on the U.S. Beaufort margin: 2. borehole constraints. *Geochemistry, Geophyics, Geosystems*, *17*, 4333–4353. https://doi.org/10.1002/2016GC006582

Ruppel, C. D., & Kessler, J. D. (2017). The interaction of climate change and methane hydrates. *Review of Geophysics*, *55*(1), 126–168. https://doi.org/10.1002/2016RG000534

Saunois, M., Stavert, A. R., Poulter, B., Bousquet, P., Canadell, J. G., Jackson, R. B., et al. (2020). The global methane budget 2000–2017. *Earth System Science Data*, *12*(3), 1561–1623. https://doi.org/10.5194/essd-12-1561-2020

Sayedi, S. S., Abbott, B. W., Thornton, B. F., Frederick, J. M., Vonk, J. E., Overduin, P., et al. (2020). Subsea permafrost carbon stocks and climate change sensitivity estimated by expert assessment. *Environmental Research Letters*, *15*(12), 124075. https://doi.org/10.1088/1748-9326/abcc29

Schirrmeister, L., Grigoriev, M., Strauss, J., Grosse, G., Overduin, P. P., Kholodov, A., et al. (2018). Sediment characteristics of a thermokarst lagoon in the northeastern Siberian Arctic (Ivashkina Lagoon, Bykovsky Peninsula). *arktos*, *4*. https://doi.org/10.1007/s41063-018-0049-8

Sellmann, P. V., Delanney, A. J., & Arcone, S. A. (1989). *Coastal submarine permafrost and bedrock observations using DC resistivity*. National Technical Information Service. Retrieved from https://apps.dtic.mil/sti/pdfs/ADA210784.pdf

Shakhova, N., Semiletov, I., & Chuvilin, E. (2019). Understanding the permafrost-hydrate system and associated methane releases in the Siberian Arctic Shelf. *Geosciences*, *9*(6), 251. https://doi.org/10.3390/geosciences9060251

Shakhova, N., Semiletov, I., Gustafsson, O., Sergienko, N., Lobkovsky, L., Dudarev, O., et al. (2017). Current rates and mechanisms of subsea permafrost degradation in the East Siberian Arctic Shelf. *Nature Communications*, *8*, 15872. https://doi.org/10.1038/ncomms15872

Shakhova, N., Semiletov, I., Leifer, I., Salyuk, A., Rekant, P., & Kosmach, D. (2010). Geochemical and geophysical evidence of methane release over the East Siberian Arctic Shelf. *Journal of Geophysical Research*, *115*(C8), C08007. https://doi.org/10.1029/2009JC005602

Shmelev, D., Veremeeva, A., Kraev, G., Kholodov, A., Spencer, R. G., Walker, W. S., & Rivkina, E. (2017). Estimation and sensitivity of carbon storage in permafrost of north-eastern Yakutia. *Permafrost and Periglacial Processes*, *28*(2), 379–390. https://doi.org/10.1002/ppp.1933

Stephani, E., Drage, J., Miller, D., Jones, B. M., & Kanevskiy, M. (2020). Taliks, cryopegs, and permafrost dynamics related to channel migration, Colville River Delta, Alaska. *Permafrost and Periglacial Processes*, *31*(2), 239–254. https://doi.org/10.1002/ppp.2046

Strauss, J., Schirrmeister, L., Grosse, G., Fortier, D., Hugelius, G., Knoblauch, C., et al. (2017). Deep Yedoma permafrost: A synthesis of depositional characteristics and carbon vulnerability. *Earth-Science Reviews*, *172*, 75–86. https://doi.org/10.1016/j.earscirev.2017.07.007

Strauss, J., Schirrmeister, L., Grosse, G., Wetterich, S., Ulrich, M., Herzschuh, U., & Hubberten, H.-W. (2013). The deep permafrost carbon pool of the Yedoma region in Siberia and Alaska. *Geophysical Research Letters*, *40*(23), 6165–6170. https://doi.org/10.1002/2013GL058088

Ulrich, M., Grosse, G., Strauss, J., & Schirrmeister, L. (2014). Quantifying wedge-ice volumes in Yedoma and thermokarst basin deposits. *Permafrost and Periglacial Processes*, *25*(3), 151–161. https://doi.org/10.1002/ppp.1810

Vasiliev, A., Melnikov, V., Streletskaya, I., & Oblogov, G. (2017). Permafrost aggradation and methane production in low accumulative laidas (tidal flats) of the Kara Sea. *Doklady Earth Sciences*, *476*, 1069–1072. https://doi.org/10.1134/S1028334X17090203

Vest Christiansen, A., & Auken, E. (2012). A global measure for depth of investigation. *Geophysics*, *77*(4), WB171–WB177. https://doi.org/10.1190/geo2011-0393.1

Westermann, S., Schuler, T. V., Gisnås, K., & Etzelmüller, B. (2013). Transient thermal modeling of permafrost conditions in southern Norway. *The Cryosphere*, *7*(2), 719–739. https://doi.org/10.5194/tc-7-719-2013

Wild, B., Shakhova, N., Dudarev, O., Ruban, A., Kosmach, D., Tumskoy, V., et al. (2018). Organic matter across subsea permafrost thaw horizons on the East Siberian Arctic Shelf. *The Cryosphere Discuss*. https://doi.org/10.5194/tc-2018-229

Wu, Y., Nakagawa, S., Kneafsey, T. J., Dafflon, B., & Hubbard, S. (2017). Electrical and seismic response of saline permafrost soil during freeze-thaw transition. *Journal of Applied Geophysics*, *146*, 16–26. https://doi.org/10.1016/j.jappgeo.2017.08.008

Zimov, S. A., Schuur, E. A., & Chapin, F. S. (2006). Permafrost and the global carbon budget. *Science*, *312*(5780), 1612–1613. https://doi.org/10.1126/science.1128908